Negative differential thermal conductance by photonic transport in electronic circuits

Shobhit Saheb Dey
Department of Physics, Indian Institute of Technology Kharagpur, Kharagpur, India 721302 and
*Quantum Research Centre, Technology Innovation Institute, Abu Dhabi, UAE**

Giuliano Timossi
NEST Istituto Nanoscienze-CNR and Scuola Normale Superiore, I-56127 Pisa, Italy

Luigi Amico
*Quantum Research Centre, Technology Innovation Institute, Abu Dhabi, UAE**
Centre for Quantum Technologies, National University of Singapore, 3 Science Drive 2, Singapore 117543
INFN-Sezione di Catania, Via S. Sofia 64, 95127 Catania, Italy
LANEF 'Chaire d'excellence', Université Grenoble-Alpes & CNRS, F-38000 Grenoble, France and
MajuLab, CNRS-UNS-NUS-NTU International Joint Research Unit, UMI 3654, Singapore

Giampiero Marchegiani
*Quantum Research Centre, Technology Innovation Institute, Abu Dhabi, UAE**
(Dated: October 23, 2022)

The negative differential thermal conductance (NDTC) provides the key mechanism for realizing thermal transistors. This exotic effect has been the object of an extensive theoretical investigation, but the implementation is still limited to a few specific physical systems. Here, we consider a simple circuit of two electrodes exchanging heat through electromagnetic radiation. We theoretically demonstrate that the existence of an optimal condition for power transmission, well-known as impedance matching in electronics, provides a natural framework for engineering NDTC: the heat flux is reduced when the temperature increase is associated to an abrupt change of the electrode's impedance. As a case study, we numerically analyze a hybrid structure based on thin-film technology, in which the increased resistance is due to a superconductor-resistive phase transition. For typical metallic superconductors operating below 1K, NDTC reflects in a temperature drop of the order of a few mK by increasing the power supplied to the system. Our numerical work draws new routes for implementing a thermal transistor in nanoscale circuits.

The development of quantum technologies is one of the main driving forces of the current physical research[1,2]. In many implementations of this discipline, device miniaturization and low noise requirement have motivated an intense theoretical investigation and experimental activity on thermal transport in nanoscale solid-state devices[3–9]. In this direction, as a combined effect of non-equilibrium thermal fluctuations and non-linear response, physical systems in which the heat flow $\dot{Q}$ decreases by increasing temperature gradients, i.e., $d\dot{Q}/dT < 0$ can be realized. In these regimes, the system is characterized by a Negative Differential Thermal Conductance (NDTC)[10]. Exploring the physical meaning of the NDTC regime defines a certainly interesting line of basic research[11–14]. At the same time, such effect allows to configure and fabricate new devices based on NDTC. An important case study in this context is provided by the thermal transistor introduced fifteen years ago by Casati and coworkers[10]. Over the years, several proposals for the implementation of thermal transistors and similar devices have been put forward, with technologies ranging from phononics[15], superconducting junctions[16,17], electrochemical cells [18] to near-field devices[19–23]. Even though great efforts have been devoted to the problem, engineering of NDTC in physical systems is still a challenging task, with only few experimental observations in specific systems being carried out [24–26]. In our work, we will show how a circuit approach to photon-mediated thermal transport can provide a general route for NDTC engineering. In our logic, we rely on a specific "resonant" property holding for the thermal transmission: The electromagnetic power turns out to be optimally transmitted between two circuital elements if a certain impedance matching condition is fulfilled[27]. Starting from this condition, we impart an abrupt impedance mismatch by a temperature change. We shall see that such protocol can lead to NDTC. After a general discussion of the mechanism, we present a quantitative investigation in a realistic platform in which the impedance mismatch is achieved through the normal-to-superconductor phase transition. We note that the photonic heat transport between two normal metals has been recently investigated in different experiments[28–33], where superconducting elements are exploited to realize a tunable coupling, both in the classical and in the quantum regime[32,34]. Here, we investigate photon-mediated heat transport in superconductors that, because of their impedance's strong temperature dependence, provide important examples of coherent networks in which nonlinear transport effects can take place[23,35–38].

We consider the scheme depicted in Fig. 1(a). The system is composed of two electrodes, denoted as source (S) and drain (D), electrically connected through wires

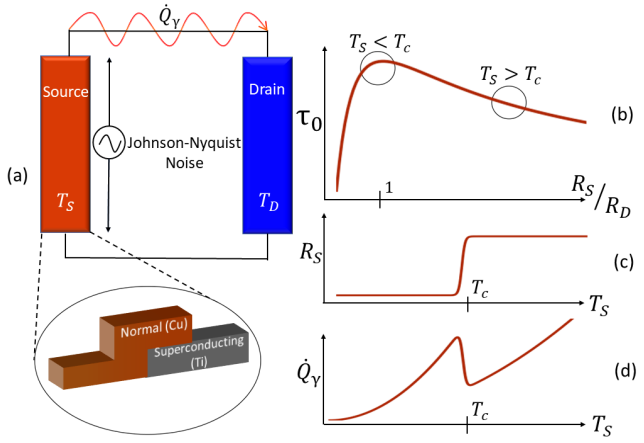

FIG. 1. NDTC in photonic transport. (a) Circuit scheme: source and drain electrode are connected through a lossless line. In the presence of a thermal gradient, heat is transferred through a photon-mediated mechanism. In the blow-up, we show the implementation discussed in the second part of the manuscript, where the source is given as a series of a normal metal and a superconductor. (b) Power transfer coupling coefficient between two normal resistors R_S and R_D. The transmission is maximum for $R_S = R_D$ (impedance matching condition). (c) Sharp increase of the source resistance due to a phase-change occuring at the temperature T_c.
(d) Resulting NDTC in the photon-mediated heat current.

of negligible losses. For the sake of generality, we follow a lumped parameters approach valid at low temperatures for photons wavelengths larger than the size of the typical circuit element[39]. We assume that the lead S is in thermal equilibrium with temperature T_S, while the drain resides at temperature T_D. When a thermal gradient is present, i.e., for $T_S \neq T_D$, heat is exchanged between the two elements. More precisely, the heat current generated due to electromagnetic fluctuations can be accounted for by means of the fluctuation-dissipation theorem[40]. The Johnson-Nyquist voltage noise density in the source reads[41,42] $S_V(\omega) = 4\omega \mathrm{Re}\,[Z_S(\omega, T_S)][n(\omega, T_S) + 1/2]$, where ω is the photon energy, $n(\omega, T) = [e^{\omega/(k_B T)} - 1]^{-1}$ is the Bose distribution, and $Z_S(\omega, T_S)$ is the source's impedance. The corresponding noise current in the circuit is $S_I(\omega) = S_V(\omega)/|Z_{\rm tot}|^2$, where $Z_{\rm tot} = Z_S(\omega, T_S) + Z_D(\omega, T_D)$ is the total impedance of the circuit, and hence the power density dissipated in the drain is $S_P(\omega) = \mathrm{Re}\,[Z_D(\omega, T_D)]S_I(\omega)$. The total power transferred is obtained by integrating over the photon frequency $\nu = \omega/h$ (h is the Planck's constant), giving

$$\dot{Q}_{S\to D}(T_S, T_D) = \frac{1}{h}\int_0^\infty \omega\tau(\omega, T_S, T_D)\left[n(\omega, T_S) + \frac{1}{2}\right] d\omega, \tag{1}$$

where the effective photon transmission coefficient has been identified as[42–44]:

$$\tau(\omega, T_S, T_D) = 4\frac{\mathrm{Re}[Z_S(\omega, T_S)]\mathrm{Re}[Z_D(\omega, T_D)]}{|Z_S(\omega, T_S) + Z_D(\omega, T_D)|^2}. \tag{2}$$

The net power transmitted is then obtained by subtracting the heat current $\dot{Q}_{D\to S}$ flowing from the drain to the source, i.e., $\dot{Q}_\gamma = \dot{Q}_{S\to D} - \dot{Q}_{D\to S}$. Due to symmetry, $\dot{Q}_{D\to S}$ is simply obtained by exchanging $S \leftrightarrow D$ in Eq. (1), yielding the following expression for $\dot{Q}_\gamma$[28,44]:

$$\dot{Q}_\gamma(T_S, T_D) = \frac{1}{h}\int_0^\infty \omega\tau(\omega, T_S, T_D)[n(\omega, T_S) - n(\omega, T_D)]\, d\omega. \tag{3}$$

In this setting, a NDTC can be achieved, for instance, when $\dot{Q}_\gamma$ *decreases* by increasing T_S for a fixed value of $T_D < T_S$. To give a simplified view, we first discuss the case where Z_S, Z_D have no reactive components and do not depend on the photon energy, i.e., $Z_S(\omega, T_S) = R_S(T_S)$ and $Z_D(\omega, T_D) = R_D(T_D)$. In this case, the integral in Eq. (3) can be explicitly evaluated as $\dot{Q}_\gamma(T_S, T_D) = \tau_0(R_S/R_D)\pi^2 k_B^2(T_S^2 - T_D^2)/(6h)$, where $\tau_0(x) = 4x/(x+1)^2$. In this expression the T^2 dependence of the heat current expresses blackbody radiation in 1D, characterized by a modified Stefan-Boltzmann constant $\sigma_{SB}^{1D} = \pi^2 k_B^2/(3h)$[4546]. The one-dimensional nature of the transport stems from the topology of the electrical circuit which connects the two elements, where the radiated photons are transmitted. The coupling coefficient τ_0 characterizes the efficiency of the power transmission, related to the relative dissipation in each element.

The key property that we use to engineer the NDTC is the non monotonous behaviour of the transmission τ_0 as function of the resistance ratio (R_S/R_D); in particular τ_0 results to be maximum at the impedance matching condition, i.e., for $R_S = R_D$[44]. This result is also known in the literature as the maximum power transfer theorem: it expresses a general statement on optimal power transfer between two elements, ranging from mechanical collisions to electromagnetic phenomena (such as the one investigated here)[47,48]. We consider a source electrode characterized by a resistance which depends sharply on the temperature around the critical value T_c, i.e., $R_S = R_D$ for $T < T_c$ and $R_S \gg R_D$ for $T > T_c$ (see Fig. 1(c)). As a consequence, the transmission τ_0 is reduced from unity (for $T < T_c$, being $R_S = R_D$) to a value much smaller than one ($T < T_c$, with $R_S/R_D \gg 1$) when the temperature is increased from $T < T_c$ to $T > T_c$, hence making $\dot{Q}_\gamma$ to decrease by increasing T_S in the vicinity of T_c - Fig. 1 (d). Note that at larger values of the source temperature the heat conductance is again positive, being the transmission approximately constant for $T > T_c$.

Now we discuss a possible scheme for the detection and implementation of NDTC. To mimic the sharp resistance increase of Fig. 1c, we exploit a superconducting to normal phase transition[49]. The drain electrode is a normal resistor with resistance R_D. We assume the source is composed of a series of a normal element (with resistance $R_N = R_D$ to ensure impedance matching) and a superconducting element, connected through a clean contact of negligible resistance (see Fig. 1a)[50]. The clean contact can be achieved through electrode beam evap-

oration of the two films in a ultra-high-vacuum chamber. Below the superconducting critical temperature, the dissipation in the superconductor is negligible, giving $\mathrm{Re}\left[Z_S(\omega,T_S)\right] \sim R_D$, whereas $\mathrm{Re}\left[Z_S(\omega,T_S)\right] = R_D + R_0$ for $T > T_c$, where R_0 is the resistance of the superconducting element in the normal state. We choose to operate in the sub-Kelvin regime, where the photonic heat current is more relevant to the thermal equilibration[36,38,42]. On the material side, we consider thin metallic films which can be deposited through electron-beam evaporation, such as Titanium (Ti) as the superconductor (with typical critical temperature in the range $0.3 - 0.5$ K[51,52], we set $T_c = 0.4$K in our calculations) and copper (Cu) for the normal conducting elements. The wires can be realized with superconducting aluminum (Al), which displays higher critical temperature than Ti[53], and therefore can account for realizing lossless lines. Indeed, the dissipation in the wire is exponentially suppressed at low temperatures due to the presence of the superconducting gap. The kinetic inductance contribution can be optimized by a suitable geometry design. At the same time, direct conduction of heat between the electrodes and the wire is suppressed by Andreev mirroring.[38]. For simplicity, we neglect the interfacial resistance between the wire and the two electrodes: this resistance reduces the transmitted heat current by increasing the real part of $Z_{\rm tot}$, but does not significantly affected the phenomenology discussed below.

We start by discussing the photon-mediated heat transport. In our setup, the impedance of the two leads are $Z_S(\omega,T_S) = R_D + Z_0(\omega,T_S)$, and $Z_D(\omega,T_S) = R_D$. As recently experimentally demonstrated[52], the complex impedance of Ti can be modeled within the Mattis-Bardeen theory[54], valid for Bardeen-Cooper-Schrieffer (BCS) superconductors. More precisely, the complex impedance reads $Z_0(\omega,T_S) = R_0[\sigma_1(\omega,T_S) - \iota\sigma_2(\omega,T_S)]^{-1}$, where the real ($\sigma_1$) and the imaginary ($\sigma_2$) parts of the complex conductivity (scaled to the normal conductivity) are expressed by:

$$\sigma_1(\omega,T) = \frac{2}{\omega}\int_{\Delta}^{\infty} \nu(E,E')[f(E,T) - f(E',T)]\,dE - \frac{\Theta(\omega-2\Delta)}{\omega}\int_{\Delta-\omega}^{-\Delta} \nu(E,E')[1-2f(E',T)]\,dE, \tag{4}$$

$$\sigma_2(\omega,T) = \frac{1}{\omega}\int_{-\Delta,\Delta-\omega}^{\Delta} |\nu(E,E')|[1-2f(E',T)]\,dE. \tag{5}$$

Above, $\Theta(x)$ is the Heaviside-step function, $E' = E+\omega$, $f(E,T) = [e^{E/(k_BT)}+1]^{-1}$ is the Fermi function, and we introduced the function[55]

$$\nu(E,E') = \frac{EE'+\Delta^2}{\sqrt{E^2-\Delta^2}\sqrt{E'^2-\Delta^2}}. \tag{6}$$

The superconducting gap is approximately given by $\Delta(T) = \Delta_0 \tanh(1.74\sqrt{T_c/T-1})$ [56] for $T \le T_c$ ($\Delta = 0$ for $T \ge T_c$) where $\Delta_0 = 1.76 k_B T_c$, according to the BCS theory. The dissipative processes in the superconductor are given by thermally excited quasiparticles (first integral of Eq. (4)) or through pair-breaking processes due to photon absorption that may occur for $\omega > 2\Delta$ (second integral of Eq. (4)). The imaginary part of the conductivity Eq. (5) gives the kinetic inductance of the superconducting film.

Figure 2a displays $\dot{Q}_\gamma$ as a function of the source temperature T_S, for $T_D = 30$ mK and different values of the ratio $r = R_0/R_D$. Notably, the evolution is non-monotonic with T_S, and the system displays NDTC for source temperatures approximately in the range around [350 mK, 400 mK]. Upon increasing R_0, the photonic heat current decreases. Here the reduction of $\dot{Q}_\gamma$ with R_0 for $T > T_c$ arises from suppression of $\tau_0(x)$ for $x > 1$, while for $T < T_c$ it is related to the imaginary part of the $Z_S(\omega,T_S)$ i.e., kinetic inductance. To analyze such a feature, we focus on the temperature dependence of τ. We define an average transmission $\bar{\tau}(T_S) = (2\Delta_0)^{-1}\int_0^{2\Delta_0}\tau(\omega,T_S)d\omega$[57]. Figure 2b displays $\bar{\tau}$ as a function of the source temperature T_S, for the same values of r as in Fig. 2a. The transmission is monotonically decreasing with T_S, being maximum at $T_S \ll T_c$, i.e., $\tau_{\rm max} = \bar{\tau}(T_S \to 0)$, and constant for $T_S \ge T_c$, with $\tau_{\rm min} = 4(1+r)/(2+r)^2$. Differently from the idealized situation displayed in Fig. 1, $\tau < 1$ even at low temperatures. This behaviour is due to the non-negligible kinetic inductance of the superconductor, which reduces τ (see Eq. (2)). Hence, even though an increase of R_0 turns out always beneficial in the schematics of Fig. 1b, in the realistic case, an arbitrarily large value of R_0 may hinder the NDTC behavior as also seen in Fig. 2a. Indeed, $\tau_{\rm max}$ and $\tau_{\rm min}$ decreases monotonically as a function of r, as displayed in Fig. 2c (solid curves). Notably, the relative transmission modulation, defined as $(\tau_{\rm max}-\tau_{\rm min})/\tau_{\rm max}$, grows monotonically with r, and it is approximately saturating to $1 - 8/\pi^2 \sim 0.19$ for $r \sim 10$ (see dashed curve in Fig. 2c)[58]. As a result, the phenomenology of NDTC is well displayed for values of r in the range [10,100].

In Fig. 2d, we display $\dot{Q}_\gamma$ as a function of T_S for $r = 36$ and different values of T_D. For a given value of the source temperature, the heat current typically decreases by increasing T_D, due to the reduction of the thermal gradient. Notably, the NDTC phenomenology for source temperatures $T_S \lesssim T_c$ is robust even with a sizeable change of the drain temperature. This feature is crucial for the detection of the NDTC discussed below.

In the above computations, we characterized the photon-mediated thermal transport as a function of the temperatures of the source for a selected values of the drain temperature. However, in an actual experiment, the temperatures T_S and T_D are not directly controlled. Instead, power is injected into the system and the temperature T_S, T_D are the result of the power balance in each electrode[9]. More precisely, experiments based on low-temperature superconducting thin films are typically well described within the quasi-equilibrium regime[3,6].

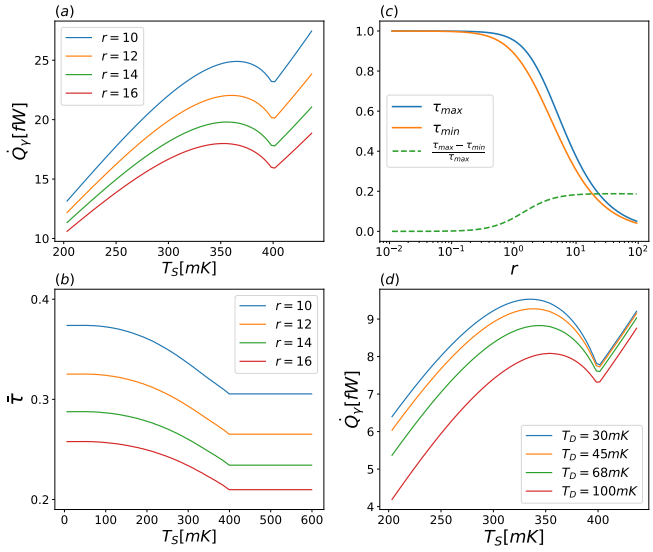

FIG. 2. NDTC in the specific implementation based on low-temperature superconductors. (a) $\dot{Q}_\gamma$ vs T_S with $T_D = 30$mK for different values of $r = R_0/R_D$. NDTC appears for source temperatures T_S around $(350\text{mK}, 400\text{mK})$, (b) Energy averaged thermal transmission $\bar{\tau}$ vs T_S for the same values of r as in (a), (c) τ_{max}, τ_{min} and their relative difference as function of r showing favourable operating region to observe NDTC, (d) $\dot{Q}_\gamma$ vs T_S for $r = 36$ and different values of T_D.

Namely, in each electrode, quasiparticles and phonons can be treated as separate subsystems, which may thermalize to different temperatures, since the electron-phonon scattering rate slows down at very low temperatures.

The thermal exchanges in our system are schematically depicted in Fig. 3a. We assume that the phonons in each part of the device are well thermalized to the substrate temperature ($T_p \sim 30$ mK set by the cryogenic dilution fridge). Due to the clean contact between Ti and Cu, we neglect any potential small thermal gradient in the source electrode, characterizing the electron (in the normal metal) and the quasiparticle (in the superconductor) subsystem with a single temperature T_S. This approximation is valid for layers with dimensions smaller than the thermal healing length associated with electron-phonon interaction, which we estimate in the range of tens to hundreds of μm[3]. The electronic temperature of the drain is given by T_D. When power $P_{\rm in}$ is injected in the source, the source temperature increases $T_S > T_p$, producing photon-mediated exchange $\dot{Q}_\gamma$ with the drain. At the same time, heat is exchanged with the phononic bath both in the normal ($\dot{Q}_N$) and in the superconducting ($\dot{Q}_{Sc}$) parts of the device. At the steady state condition, in each element the ingoing heat current must be equal to the outgoing heat current, giving:

$$\begin{cases} P_{\rm in} = \dot{Q}_\gamma(T_S, T_D) + \dot{Q}_N(T_S, T_p) + \dot{Q}_{Sc}(T_S, T_p) \\ \dot{Q}_\gamma(T_S, T_D) = \dot{Q}_N(T_D, T_p) \end{cases} \tag{7}$$

The electron-phonon coupling in each Cu lead is given by $\dot{Q}_N(T, T_p) = \Sigma_{\rm Cu}\mathcal{V}_N(T^5 - T_p^5)$, where $\mathcal{V}_N$ is the volume of each copper electrode and $\Sigma_{\rm Cu} = 3 \times 10^9 \text{W m}^{-3}\text{K}^{-5}$ is the material dependent electron-phonon coupling constant[3]. For the superconductor, the electron-phonon interaction reads[59,60]

$$\dot{Q}_{Sc}(T_S, T_p) = \lambda_s \int_0^\infty d\omega\omega^3[n(\omega, T_S) - n(\omega, T_p)]\mathcal{F}(\omega, T_S), \tag{8}$$

where $\lambda_s = \Sigma_{\rm Ti}\mathcal{V}/(24\zeta(5)k_B^5)$ and

$$\mathcal{F}(\omega, T_S) = \int_{-\infty}^\infty dE\rho(E)\rho(E')\left(1 - \frac{\Delta^2}{EE'}\right) [f(E, T_S) - f(E', T_S)] \tag{9}$$

with $E' = E + \omega$. Above, $\Sigma_{\rm Ti} = 1.3 \times 10^9 \text{W m}^{-3}\text{K}^{-5}$ is the coupling coefficient[3], $\mathcal{V}$ is the volume of the superconducting lead, $\zeta(z)$ is the Riemann-Zeta function, and $\rho(E) = |E|\theta(|E| - \Delta)/\sqrt{E^2 - \Delta^2}$ is the BCS density of states. For given values of the phonon temperature T_p

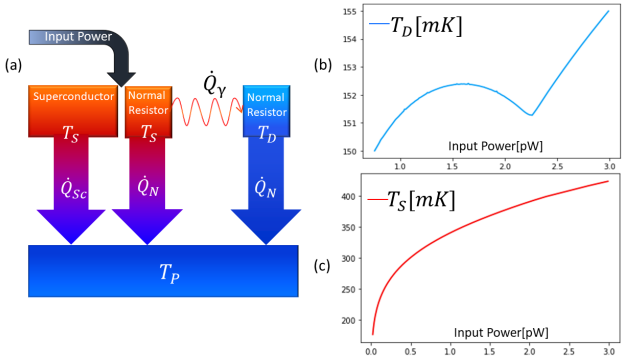

FIG. 3. Thermal balance and source and drain steady-state temperatures. (a) Heat flow diagram: input power is provided to the source, and losses due to electron-phonon coupling are included. (b) Steady state temperature of the drain T_D vs input power $P_{\rm in}$, showing negative differential characteristics with respect to $P_{\rm in}$. (c) Steady state temperature of the source T_S vs $P_{\rm in}$, showing a monotonic increase with input power. Parameters: $T_p = 30$mK, $\rho_{\rm Cu} = 3\ \mu\Omega\cdot\text{cm}$[61], $l_{\rm Cu} = 2\ \mu$m, $\mathcal{A}_{\rm Cu} = 700 \times 30\ \text{nm}^2$, $\rho_{\rm Ti} = 30\ \mu\Omega\cdot\text{cm}$[62], $l_{\rm Ti} = 6\ \mu$m, $\mathcal{A}_{\rm Ti} = 700 \times 25\ \text{nm}^2$, where $\rho, l, \mathcal{A}$ are the normal state resistivity, the length and the cross section of the films, respectively.

and the input power $P_{\rm in}$ Eq. (7) is a nonlinear system of integro-algebraic equations in the two-variables for T_S and T_D.

Figure 3(b)-(c) displays the solution of Eq. (7), obtained through a Newton-Raphson optimization algorithm, as a function of the input power $P_{\rm in}$. Notably, while T_S increases monotonously with $P_{\rm in}$ (see Fig. 3(c)), the drain temperature T_D decreases for input power around the range $[1.5, 2.25]$ pW (see Fig. 3(b)). This behavior is a signature of NDTC in the photonic channel. Indeed, when T_S is close to T_c (400 mK) the heat

exchange is reduced by increasing $P_{\rm in}$, in agreement with our previous discussion, resulting in a decrease of T_D due to the second equation in Eq. (7).

In summary, we investigated the Negative Differential Thermal Conductance (NDTC) in the photonic heat transport between two electrodes, within a lumped circuital approach. We rely on a photon resonant transmission that, in analogy of the electronic principle of impedance matching[27], minimize the loss in the heat transmission. We demonstrated how such resonant transmission can be exploited as a reference point to realize NDTC. An abrupt impedance mismatch causes a reduction of the heat flow that can be transmitted among the two electrodes, and therefore the differential conductance is negative. In the second part of the paper, we focus on a specific design based on low-temperature superconductor, that can be realized with the state-of-the-art nano-fabrication techniques. Our calculations shows that the effect leads to temperature drops larger than 1 mK. Thus, the predicted NDTC phenomenology can be identified with well-established normal-insulator-superconductor junction thermometric techniques, with typical uncertainty of 40 μK[29]. Our work provides a general protocol for engineering NDTC in electric circuits where heat is exchanged through electromagnetic radiation. In this respect, superconducting circuits certainly provide a promising platform. The general nature of the maximum power transfer condition, though, may trigger investigations of NDTC on a wider variety of physical implementations. Improved performance in terms of the operating temperature range or size of the temperature drop with the use of alternative materials and phase transitions. These topics could be subject of future research.

Acknowledgements. We thank Gianluigi Catelani, and Alessandro Braggio for fruitful discussions.

* shobhitsahebdey@iitkgp.ac.in

[1] J. P. Dowling and G. J. Milburn, Phil. Trans. R. Soc. A. **361**, 1655 (2003).
[2] A. Acín, I. Bloch, H. Buhrman, T. Calarco, C. Eichler, J. Eisert, D. Esteve, N. Gisin, S. J. Glaser, F. Jelezko, *et al.*, New J. Phys. **20**, 080201 (2018).
[3] F. Giazotto, T. T. Heikkilä, A. Luukanen, A. M. Savin, and J. P. Pekola, Rev. Mod. Phys. **78**, 217 (2006).
[4] Y. Dubi and M. Di Ventra, Rev. Mod. Phys. **83**, 131 (2011).
[5] G. E. W. Bauer, E. Saitoh, and B. J. van Wees, Nat. Mater. **11**, 391 (2012).
[6] J. T. Muhonen, M. Meschke, and J. P. Pekola, Rep. Prog. Phys. **75**, 046501 (2012).
[7] D. G. Cahill, P. V. Braun, G. Chen, D. R. Clarke, S. Fan, K. E. Goodson, P. Keblinski, W. P. King, G. D. Mahan, A. Majumdar, H. J. Maris, S. R. Phillpot, E. Pop, and L. Shi, Appl. Phys. Rev. **1**, 011305 (2014).
[8] B. Song, A. Fiorino, E. Meyhofer, and P. Reddy, AIP Adv. **5**, 053503 (2015).
[9] A. Fornieri and F. Giazotto, Nat. Nanotechnol. **12**, 944 (2017).
[10] B. Li, L. Wang, and G. Casati, Appl. Phys. Lett. **88**, 143501 (2006).
[11] N. Yang, N. Li, L. Wang, and B. Li, Phys. Rev. B **76**, 020301 (2007).
[12] D. He, B.-q. Ai, H.-K. Chan, and B. Hu, Phys. Rev. E **81**, 041131 (2010).
[13] D. He, S. Buyukdagli, and B. Hu, Phys. Rev. B **80**, 104302 (2009).
[14] J. Hu and Y. P. Chen, Phys. Rev. E **87**, 062104 (2013).
[15] N. Li, J. Ren, L. Wang, G. Zhang, P. Hänggi, and B. Li, Rev. Mod. Phys. **84**, 1045 (2012).
[16] A. Fornieri, G. Timossi, R. Bosisio, P. Solinas, and F. Giazotto, Phys. Rev. B **93**, 134508 (2016).
[17] M. Zare, Supercond. Sci. Technol. **32**, 115002 (2019).
[18] A. Sood, F. Xiong, S. Chen, H. Wang, D. Selli, J. Zhang, C. J. McClellan, J. Sun, D. Donadio, Y. Cui, E. Pop, and K. E. Goodson, Nat. Commun. **9**, 4510 (2018).
[19] C. R. Otey, W. T. Lau, and S. Fan, Phys. Rev. Lett. **104**, 154301 (2010).
[20] L. Zhu, C. R. Otey, and S. Fan, Appl. Phys. Lett. **100**, 044104 (2012).
[21] P. Ben-Abdallah and S.-A. Biehs, Phys. Rev. Lett. **112**, 044301 (2014).
[22] S.-A. Biehs, R. Messina, P. S. Venkataram, A. W. Rodriguez, J. C. Cuevas, and P. Ben-Abdallah, Rev. Mod. Phys. **93**, 025009 (2021).
[23] E. Moncada-Villa and J. C. Cuevas, Phys. Rev. Applied **15**, 024036 (2021).
[24] M. A. Kats, R. Blanchard, S. Zhang, P. Genevet, C. Ko, S. Ramanathan, and F. Capasso, Phys. Rev. X **3**, 041004 (2013).
[25] K. Ito, K. Nishikawa, H. Iizuka, and H. Toshiyoshi, Appl. Phys. Lett. **105**, 253503 (2014).
[26] V. c. v. Musilová, T. c. v. Králík, T. c. v. Fořt, and M. Macek, Phys. Rev. B **99**, 024511 (2019).
[27] C. J. Kikkert, "Rf electronics: design and simulation," (2013).
[28] M. Meschke, W. Guichard, and J. P. Pekola, Nature **444**, 187 (2006).
[29] A. Ronzani, B. Karimi, J. Senior, Y.-C. Chang, J. T. Peltonen, C. Chen, and J. P. Pekola, Nat. Phys. **14**, 991 (2018).
[30] J. Senior, A. Gubaydullin, B. Karimi, J. T. Peltonen, J. Ankerhold, and J. P. Pekola, Commun. Phys. **3**, 40 (2020).
[31] O. Maillet, D. Subero, J. T. Peltonen, D. S. Golubev, and J. P. Pekola, Nat. Commun. **11**, 4326 (2020).
[32] G. Thomas, J. P. Pekola, and D. S. Golubev, Phys. Rev. B **100**, 094508 (2019).
[33] A. Gubaydullin, G. Thomas, D. S. Golubev, D. Lvov, J. T. Peltonen, and J. P. Pekola, Nat. Commun. **13** (2022), 10.1038/s41467-022-29078-x.
[34] B. Karimi, J. P. Pekola, M. Campisi, and R. Fazio, Quantum Sci. Technol. **2**, 044007 (2017).
[35] E. Nefzaoui, K. Joulain, J. Drevillon, and Y. Ezzahri, Appl. Phys. Lett. **104**, 103905 (2014).
[36] R. Bosisio, P. Solinas, A. Braggio, and F. Giazotto, Phys. Rev. B **93**, 144512 (2016).

[37] J. Ordonez-Miranda, K. Joulain, D. De Sousa Meneses, Y. Ezzahri, and J. Drevillon, J. Appl. Phys. **122**, 093105 (2017).

[38] G. Marchegiani, A. Braggio, and F. Giazotto, Appl. Phys. Lett. **118**, 022602 (2021).

[39] At $T = 1$K, the photon thermal wavelength is $\lambda = hc/(k_B T) = 1.4$ cm.

[40] E. M. Lifshitz and L. P. Pitaevskii, *Statistical physics: theory of the condensed state*, Vol. 9 (Elsevier, 2013).

[41] H. Nyquist, Phys. Rev. **32**, 110 (1928).

[42] D. R. Schmidt, R. J. Schoelkopf, and A. N. Cleland, Phys. Rev. Lett. **93**, 045901 (2004).

[43] T. Ojanen and A.-P. Jauho, Phys. Rev. Lett. **100**, 155902 (2008).

[44] L. M. A. Pascal, H. Courtois, and F. W. J. Hekking, Phys. Rev. B **83**, 125113 (2011).

[45] P. T. Landsberg and A. D. Vos, J. Phys. A: Math. Gen. **22**, 1073 (1989).

[46] The additional factor 1/2 in the heat current is due to the polarisation of the photons in the conductors.

[47] M. Harrison, Phys. Educ. **48**, 207 (2013).

[48] K. Atkin, Phys. Educ. **48**, 616 (2013).

[49] M. Tinkham, *Introduction to superconductivity* (Dover Publications, Mineola, New York, 2004).

[50] For simplicity, we neglect the superconducting proximity effect between the two elements[63].

[51] M. C. Steele and R. A. Hein, Phys. Rev. **92**, 243 (1953).

[52] M. Thiemann, M. Dressel, and M. Scheffler, Phys. Rev. B **97**, 214516 (2018).

[53] The bulk critical temperature of Al is $T_c^{\mathrm{Al}} = 1.2$ K and larger for thin films (up to $3K$ for 3 nm thick films).

[54] D. C. Mattis and J. Bardeen, Phys. Rev. **111**, 412 (1958).

[55] In Eq. (5), $\sqrt{E^2 - \Delta^2}$ is purely imaginary and should be intended as $\sqrt{\Delta^2 - E^2}$ due to the presence of the absolute value. The lower limit of integration is the maximum between $-\Delta$ and $\Delta - \omega$.

[56] This approximate expression gives an accurate description for the temperature dependence of the gap, with an error smaller than 3% for every temperature.

[57] The cutoff at $2\Delta_0$ is related to the fact that we are mainly interested in temperatures $T_S \leq T_c$.

[58] This value is obtained by integration at $T = 0$, by using the low frequency approximation $Z_0(\omega, T_S = 0) \sim i\omega R_0/(\pi\Delta_0)$.

[59] A. V. Timofeev, C. P. García, N. B. Kopnin, A. M. Savin, M. Meschke, F. Giazotto, and J. P. Pekola, Phys. Rev. Lett. **102**, 017003 (2009).

[60] V. F. Maisi, S. V. Lotkhov, A. Kemppinen, A. Heimes, J. T. Muhonen, and J. P. Pekola, Phys. Rev. Lett. **111**, 147001 (2013).

[61] K. L. Viisanen and J. P. Pekola, Phys. Rev. B **97**, 115422 (2018).

[62] G. De Simoni, F. Paolucci, P. Solinas, E. Strambini, and F. Giazotto, Nat. Nanotechnol. **13**, 802 (2018).

[63] B. Pannetier and H. Courtois, J. Low Temp. Phys. **118**, 599 (2000).